Journal of Biomolecular NMR, 4 (1994) 349–366
ESCOM

J-Bio NMR 183

^{1}H, ^{15}N and ^{13}C resonance assignments, secondary structure, and the conformation of substrate in the binary folate complex of *Escherichia coli* dihydrofolate reductase

Christopher J. Falzone[a], John Cavanagh[b], Marlon Cowart[a], Arthur G. Palmer III[b], C. Robert Matthews[a], Stephen J. Benkovic[a] and Peter E. Wright[b,*]

[a]*Pennsylvania State University, Department of Chemistry and the Center for Biomolecular Structure and Function, University Park, PA 16802, U.S.A.*

[b]*Department of Molecular Biology, The Scripps Research Institute, 10666 North Torrey Pines Road, La Jolla, CA 92037, U.S.A.*

Received 17 September 1993
Accepted 19 November 1993

Keywords: 3D NMR; Dihydrofolate reductase; DHFR; Isotopic labeling; Resonance assignments

SUMMARY

By using fully ^{15}N- and $^{15}N/^{13}C$-labeled *Escherichia coli* dihydrofolate reductase, the sequence-specific ^{1}H and ^{15}N NMR assignments were achieved for 95% of the backbone resonances and for 90% of the $^{13}C^{\alpha}$ resonances in the binary folate complex. These assignments were made through a variety of three-dimensional proton-detected ^{15}N and ^{13}C experiments. A smaller but significant subset of side-chain ^{1}H and ^{13}C assignments were also determined. In this complex, only one ^{15}N or ^{13}C resonance was detected per ^{15}N or ^{13}C protein nucleus, which indicated a single conformation. Proton-detected ^{13}C experiments were also performed with unlabeled DHFR, complexed with ^{13}C-7/^{13}C-9 folate to probe for multiple conformations of the substrate in its binary complex. As was found for the protein resonances, only a single bound resonance corresponding to a productive conformation could be detected for C-7. These results are consistent with an earlier report based on ^{1}H NMR data [Falzone, C.J. et al. (1990) *Biochemistry*, **29**, 9667–9677] and suggest that the *E. coli* enzyme is not involved in any catalytically unproductive binding modes in the binary complex. This feature of the *E. coli* enzyme seems to be unique among the bacterial forms of DHFR that have been studied to date.

INTRODUCTION

Dihydrofolate reductase (5,6,7,8-tetrahydrofolate: $NADP^{+}$ oxidoreductase, EC 1.5.1.3; DHFR) catalyzes the NADPH-dependent reduction of 7,8-dihydrofolate (H_2F) to form 5,6,7,8-tetrahydrofolate (H_4F). Tetrahydrofolate is an important cofactor in the biosynthesis of purines

*To whom correspondence should be addressed.

and amino acids; consequently, DHFR is a target enzyme for the chemotherapeutic agent methotrexate and the antibacterial compounds trimethoprim and pyrimethamine. It is a monomeric protein with a molecular weight of 18 kDa and it has no prosthetic groups. A large body of information is available on this protein, including its kinetic scheme (Fierke et al., 1987) as well as several crystal structures (Bystroff and Kraut, 1991), but the enzyme displays unusual properties in solution that are of interest and amenable to study by NMR techniques. Of particular interest are various dynamic processes, e.g., the slow interconversion of protein isomers in the methotrexate (MTX) complex (Falzone et al., 1991), and the conformational fluctuations of a flexible loop in the apoprotein (Li et al., 1992). In order to characterize fully these dynamic processes and to investigate the dynamics and binding modes of substrates and inhibitors, as complete a set of ^{1}H, ^{15}N and ^{13}C NMR assignments as possible is needed. This information will also allow for a detailed description of how the binding of substrates and inhibitors influences the backbone dynamics in this protein.

There are two main consequences of the dynamic processes in DHFR. First, owing to the short T_2 relaxation times, the ^{1}H linewidths are relatively large. This causes severe overlap problems in purely homonuclear spectra and thus makes unambiguous ^{1}H assignments impossible in many cases. By combining the larger chemical shift dispersion of ^{13}C, ^{15}N, or both, with the improved resolving power of 3D NMR methods, much of the spectral overlap and degeneracy observed in purely 2D homonuclear spectra is removed. Second, for most experiments, the short relaxation times are also responsible for lower sensitivity; this arises from the decay of magnetization during the pulse sequence prior to acquisition of the signal. By using an isotopically labeled sample, it is possible to mediate coherence transfer through the relatively large ^{1}H-^{15}N, ^{1}H-^{13}C, ^{15}N-^{13}C and ^{13}C-^{13}C scalar couplings. The increased sensitivity of such experiments, compared to those relying solely on transfer through the smaller ^{1}H-^{1}H coupling, can be significant. Consequently, the use of 3D heteronuclear NMR methods are essential for assigning the spectra of DHFR, providing not only higher sensitivity in some cases, but alleviating considerable resonance congestion. 3D ^{15}N NOESY-HSQC, 3D ^{15}N TOCSY-HSQC and 3D HCCH-COSY (Ikura et al., 1991), HCCH-TOCSY (Bax et al., 1990a), ^{13}C NOESY-HSQC and HN(CO)CA (Bax and Ikura, 1991) experiments were therefore performed and analyzed for the DHFR–folate complex.

Several reports have indicated that folate may bind in two conformations to wild-type *Lactobacillus casei* DHFR: one that is productive and similar to the conformation in the *E. coli* X-ray crystal structure and another which is unproductive and similar to the MTX conformation in solution (Birdsall et al., 1989) or in the solid-state structure (Bolin et al., 1982). We have previously reported (Falzone et al., 1990) that H7 on the pterin ring of folate is found in a single conformation in solution. This conclusion relied on NOEs between H7 and the protein matrix (Ile^{5} and Ile^{94}); the corresponding conformation was found to be a productive one. In contrast, *E. coli* DHFR shows two distinct conformations of both the protein and the inhibitor in the binary

---

Abbreviations: COSY, correlated spectroscopy; 2D, 3D, two-, three-dimensional; DHFR, dihydrofolate reductase; DTT, dithiothreitol; HCCH-COSY, 3D ^{1}H-^{13}C-^{13}C-^{1}H correlation spectroscopy through $^{1}J_{CC}$ couplings; HCCH-TOCSY, 3D ^{1}H-^{13}C-^{13}C-^{1}H correlation spectroscopy through isotropic mixing of ^{13}C magnetization; H_2F, 7,8-dihydrofolate; H_4F, 5,6,7,8-tetrahydrofolate; HN(CO)CA, 3D triple-resonance NH-C^{α} correlation spectroscopy; HSQC, heteronuclear single-quantum spectroscopy; MTX, methotrexate; NOE, nuclear Overhauser effect; NOESY, two-dimensional proton nuclear Overhauser spectroscopy; 2QF-COSY, double-quantum-filtered COSY; TMP, trimethoprim; TOCSY, total correlation spectroscopy.

MTX complex (Falzone et al., 1991). This result was consistent with the binding of MTX (and not folate) to two conformers of the enzyme (E_1/E_2); these conformers were revealed by the biphasic quenching of the intrinsic enzyme fluorescence (Cayley et al., 1981). Interestingly, both human and *L. casei* DHFR show only a single bound form for the inhibitor and show no splitting of protein resonances (Carr et al., 1991; Stockman et al., 1992). In order to determine whether there are multiple enzyme conformations in solution for the *E. coli* DHFR–folate complex and to provide a more complete set of resonance assignments (^1H, ^{15}N and ^{13}C), proton-detected 2D and 3D experiments were performed with uniformly labeled ^{15}N and $^{15}N/^{13}C$ protein. To examine the potential for multiple conformations of the folate pteridine, ^1H-^{13}C 2D HSQC-NOESY experiments were acquired using a ^{13}C-7/^{13}C-9-labeled folate.

MATERIALS AND METHODS

Protein preparation and purification

A synthetic DHFR gene which overproduced protein using a modified lac promoter was constructed in the laboratory of one of us (C.R.M.) by Dr. Masa Iwakura (Iwakura and Tanaka, 1992). After transformation of the cell line NCM-533 by this plasmid, overproduction was checked in minimal media without isotopic label. Significantly better yields were obtained by using trimethoprim (TMP) in the culture mixture (10 mg/l), but a modified purification scheme was needed with this inhibitor present (see below). ^{15}N- and $^{15}N/^{13}C$-labeled DHFR were prepared by using $^{15}NH_4Cl$ and $^{15}NH_4Cl$ and ^{13}C-glucose, respectively, in a minimal medium. The minimal medium contained per liter: 6 g Na_2HPO_4, 3 g KH_2PO_4, 1 g $^{15}NH_4Cl$, 0.5 g NaCl, 0.24 g $MgSO_4$, 2 g ^{13}C-glucose, 11 mg $CaCl_2$, 50 mg ampicillin, 50 mg kanamycin, 10 mg TMP and 200 mg thiamine. Two starter cultures were made which contained $^{15}NH_4Cl$ and $^{15}NH_4Cl/^{13}C$-glucose, respectively. After an overnight growth, DHFR production was confirmed by using SDS-PAGE. The two 2-l flasks containing 1 l of minimal-$^{15}NH_4Cl$ and minimal-$^{15}NH_4Cl/^{13}C$ media were inoculated from the two respective 10-ml starting cultures; cells were harvested by centrifugation after a 14-h cell growth.

Protein purification

The protein purification was carried out as reported previously up to the MTX affinity column step (Baccanari et al., 1977; Falzone et al., 1990). The presence of TMP in the cell cultures inhibited complete DHFR binding to the MTX affinity column. This necessitated two rounds of batch binding of the protein solution to MTX resin. After 90% ammonium sulfate precipitation, the protein was taken up in ca. 10–15 ml of 50 mM phosphate buffer (pH 6) and 15–20 ml of MTX resin was introduced into a disposable 50 ml centrifuge tube. The mixture was allowed to agitate on a nutation device for 12 h at room temperature and overnight in the cold room. After the first batch-binding step, activity was detected in the supernatant even after the addition of freshly prepared MTX resin. A column was poured and the first 250 ml of wash was collected and concentrated to about 20 ml, using an Amicon concentrator with a YM3 membrane. This effluent, which contained active protein (by assay and by 12% SDS-PAGE), was cycled through a second round of batch binding with the MTX resin. DHFR was eluted from the affinity column after a high salt/high pH (1 M KCl pH 9.0) wash, using 2 mM folate in the same buffer. Nucleotides and folate were removed in the usual fashion using a DEAE-Sephacel ion-exchange

column. The protein was stored as the ammonium sulfate precipitate until use. Protein obtained in the second round of MTX resin binding was combined with the protein from the first round.

Sample preparation

The protein was spun down in an SS-34 rotor at 10 000 rpm for 30 min. After dissolving the protein in 4 ml of 25 mM phosphate buffer (pH 6.80, containing 0.5 mM EDTA and 0.5 mM DTT), the solution was dialyzed twice against 2 l of the same buffer for 12 h. The final dialysis was performed against 3 mM phosphate (pH 6.80, 0.025 mM DTT) over argon. Both the ^{15}N and the $^{15}N/^{13}C$ proteins were lyophilized and stored over argon at 4 °C until preparation of the NMR samples. Lyophilized proteins were dissolved in either 0.35 ml of 99.96% $^{2}H_2O$, 100 mM KCl or 95% H_2O/5% $^{2}H_2O$, 100 mM KCl with the final volumes being 0.45 ml. Unlabeled folic acid (J.T. Baker), which was purified before use, was added in a 1:1.3 ratio for all samples. ^{13}C-7/^{13}C-9-labeled folic acid was prepared as previously reported (Cowart et al., 1994) and was added to unlabeled DHFR in a 1:1.3 ratio. Final protein concentrations for the NMR experiments were 1.2 mM for the $^{15}N/^{13}C$ sample, 2 mM for the ^{15}N sample and 3 mM for the unlabeled DHFR sample. The pH of the protein solutions was 6.80 ± 0.1; meter readings were not corrected for isotope effects.

NMR measurements

Two-dimensional ^{1}H-^{13}C HSQC and HSQC-NOESY experiments were collected on the ^{13}C-7/^{13}C-9-labeled folate–DHFR sample with pulse sequences described previously (Bax et al., 1990b; Norwood et al., 1990). The spectral widths in F_2 and F_1 were 7042 Hz (^{1}H) and 11363 Hz (^{13}C), respectively; 4096 real points were collected in F_2 with the carrier placed on the residual $^{2}H^{1}HO$ resonance. The ^{13}C carrier was chosen to prevent folding of undesired resonances into the ^{13}C-7 frequency, but was moved near the ^{13}C-7 resonance for WALTZ-16 decoupling (Shaka et al., 1983) during acquisition. A total of 320 increments was collected in the F_1 dimension and quadrature detection was achieved using TPPI (Drobny et al., 1979; Marion and Wüthrich, 1983). After zero-filling, multiplication with an exponential window (5–8 Hz) in ω_2 and shifted Kaiser window or a Gaussian window in ω_1 and Fourier transformation, the resulting matrix consisted of 2K × 1K complex points.

The HCCH-TOCSY (Bax et al., 1990a) and constant-time HCCH-COSY (Ikura et al., 1991) experiments were collected as previously described, with the exception that a DIPSI-2 pulse train (Shaka et al., 1988) was applied for the TOCSY mixing and the 180° carbonyl pulse centered in the t_2 period was on-resonance. The ^{1}H carrier was placed at 2.26 ppm and the ^{13}C carrier at 41.4 ppm. For the HCCH-TOCSY experiment, the DIPSI-2 mixing period was 22 ms and the field strength was 10.9 kHz. These spectra were recorded in $^{2}H_2O$ at 298 K; the HN(CO)CA and the ^{15}N data were collected using 95% $^{1}H_2O$/5% $^{2}H_2O$ at 303 K with a Bruker AMX 500 spectrometer. States (States et al., 1982) or TPPI-States (Marion et al., 1989b) methods were used to achieve quadrature detection in the F_1 and F_2 dimensions and the heteronuclei were decoupled during acquisition with a GARP-1 pulse train (Shaka et al., 1985). The t_3, t_2 and t_1 data matrix consisted of 512, 32 and 128 complex points with spectral widths of 12 500, 5684 and 4000 Hz, respectively. The HNCOCA spectrum was acquired using the pulse sequence of Bax and Ikura (1991) with spectral widths in the F_3 (^{1}H), F_2 ($^{13}C^{\alpha}$) and F_1 (^{15}N) dimensions of 6757, 3017 and 1550 Hz, respectively; the data matrix before zero-filling was composed of 512, 64 and 32 complex points,

respectively. The three channels of the spectrometer were used for ^{1}H, ^{15}N and $^{13}C^{\alpha}$ pulses; a home-built fourth channel was added to the AMX console to generate carbonyl pulses. The GARP-1 pulse train was applied for ^{15}N decoupling during acquisition. Carrier frequencies were set at 8.09 ppm (^{1}H), 118 ppm (^{15}N), 177 ppm (C') and 58 ppm (C^{α}).

The 3D ^{15}N NOESY-HSQC (100 ms mixing time) and ^{15}N TOCSY-HSQC (37 ms mixing time) spectra were collected using spectral widths of 4000 Hz for ^{1}H in the F_3 dimension, 2000 Hz for ^{15}N in the F_2 dimension, and 7000 Hz for ^{1}H in the F_1 dimension and the respective data matrices consisted of $512 \times 32 \times 128$ complex points; the corresponding carrier frequencies were set at 8.09, 118 and 4.76 ppm. The ^{1}H frequency was referenced to the $^{2}H^{1}HO$ line at 4.76 ppm at 298 K and 4.73 ppm at 303 K. The ^{15}N and ^{13}C chemical shifts were referenced indirectly to liquid NH_3 and TMS using the $^{15}N/^{1}H$ frequency ratio (Live et al., 1984) or the $^{13}C/^{1}H$ frequency ratio (Bax and Subramanian, 1986).

RESULTS AND DISCUSSION

Resonance assignments

We had previously made assignments of the amino acid side chains in hydrophobic clusters by using the X-ray crystal structure (Falzone et al., 1990). The current set of assignments of the aliphatic amino acids confirms those earlier ^{1}H assignments. Of the 148 expected (^{15}N-^{1}H) amide resonances, 141 are observed in the ^{1}H-^{15}N HSQC spectrum of the uniformly labeled *E. coli* DHFR in the folate complex at pH 6.8 (Fig. 1). This is a significant improvement over the ^{1}H 2QF-COSY spectrum, which showed about 60% of the expected $C^{\alpha}H$-NH cross peaks in the fingerprint region. This difference is most likely due to the mutual cancellation of antiphase multiplet components in the 2QF-COSY cross peaks, caused by linewidths which are on the order of the active scalar coupling. The cross peaks in the HSQC spectrum are purely in-phase in both dimensions. Identification of the amino acid side-chain spin systems was made most readily by combining the results from the HCCH-COSY and HCCH-TOCSY experiments with those from the 3D ^{15}N TOCSY-HSQC experiment. In the HCCH-TOCSY spectra, complete transfer within the side-chain spin system was often detected at each ^{13}C frequency of the residue. For example, Fig. 2 presents a slice (^{13}C = 19.5 ppm) of the HCCH-TOCSY experiment that shows the correlation of various methyl resonances with the rest of their side chains for Leu^{28}, Val^{40}, Leu^{54}, Val^{72}, Val^{75}, Val^{78}, Val^{88}, Val^{93}, Val^{99}, Leu^{112}, Thr^{113} and Thr^{123}. The ^{15}N 3D TOCSY-HSQC experiment correlated almost all of the amide resonances with the α-protons and many of the β-protons. Figure 3 contains a slice (^{15}N = 121.9 ppm) taken from this experiment, illustrating the amide correlations for residues Leu^{4}, Ala^{7}, Leu^{8}, Asp^{11}, Ala^{19}, Leu^{24}, Val^{40}, Ile^{41}, Ile^{50}, Ala^{81}, Met^{92}, Ala^{107}, Tyr^{111}, Val^{119}, His^{141} and Ala^{143}. Although the 3D ^{15}N TOCSY-HSQC experiment rarely provided complete correlation of side chains, the combination of ^{13}C with the ^{15}N data sets allowed assignment of most of the side-chain resonances.

Despite the increased sensitivity in both the ^{13}C and ^{15}N proton-detected experiments, a number of β-methylene carbon and proton assignments could not be made. This is particularly obvious for isoleucine and leucine side chains, where correlation of the $C^{\alpha}H$ could be made at the ^{13}C-methyl frequencies without the corresponding $C^{\beta}H_2$ displaying detectable cross peaks in the HCCH-TOCSY experiment. For example, Fig. 2 shows a plane in the methyl region from the HCCH-TOCSY experiment where three leucine spin systems are found (residues 28, 54 and 112);

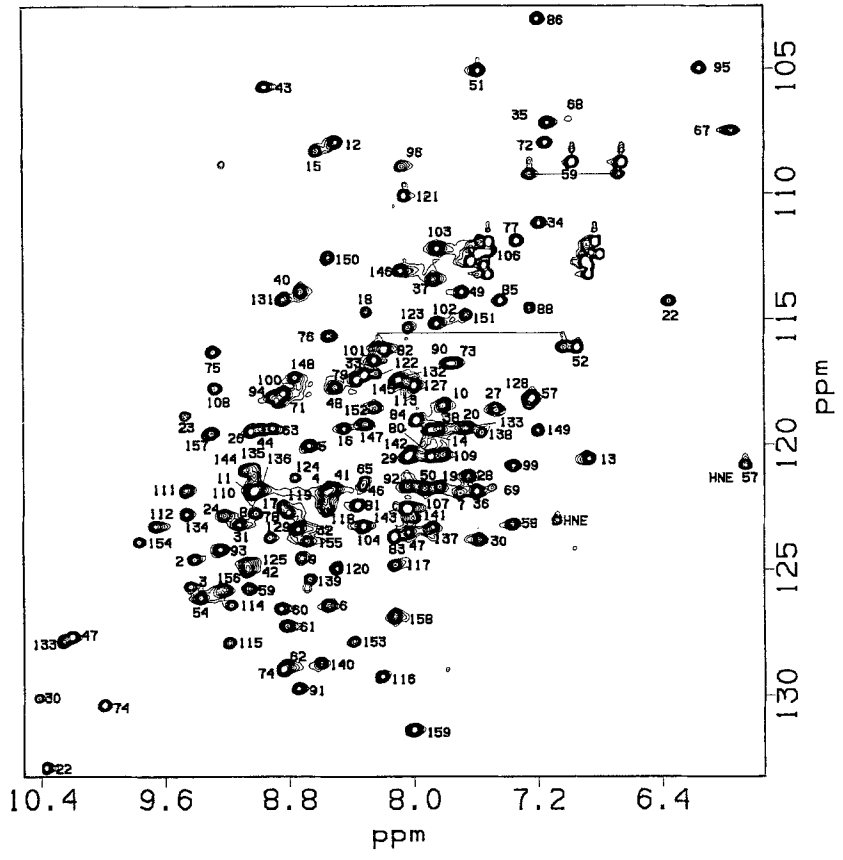

Fig. 1. 2D ^{1}H-^{15}N HSQC spectrum of uniformly ^{15}N-labeled DHFR in its folate complex, recorded at 500 MHz (^{1}H), pH 6.8, ca. 50 mM phosphate, 100 mM KCl in 95% H_2O/5% $^{2}H_2O$, 303 K. The assignments indicated in this figure were obtained using methods discussed in the Results and Discussion section. Horizontal lines are drawn for two NH_2 groups from asparagine and glutamine residues for purposes of clarification. Also indicated (as HNE) are some of the folded $N^{\varepsilon}H$ resonances of arginine side chains.

all three of these spin systems do not readily show correlation to their β-methylene protons. Correlation of the $C^{\beta}H_2$ can be made at the chemical shift of the $^{13}C^{\alpha}$ for Leu^{28} (and at the $^{13}C^{\beta}$ plane). One of the $C^{\beta}H$ of Leu^{112} may be assigned, but the ^{13}C assignment for the β-methylene remains undetected. Leu^{54} is missing both its proton and carbon assignments for the methylene group. Apparently, the large linewidths and hence, the relatively fast ^{1}H and ^{13}C relaxation rates, prevent facile assignment of the entire side chain for many residues in DHFR, using one of the most powerful proton-detected experiments.

The enhanced sensitivity of the 3D ^{15}N NOESY-HSQC enabled the sequential assignment of a considerable fraction of the backbone (Wüthrich, 1986; Clore and Gronenborn, 1989). For example, Fig. 4 displays a series of NH strips for residues 26–40, taken from various ^{15}N frequencies in the 3D NOESY-HSQC experiment; $N_iN_{(i+1)}$ NOEs are observed for residues 26–36 which comprise the αB helix (24–35) and the $\alpha_iN_{(i+1)}$ for residues 36–40 (the βB strand). For residue (i), intraresidue NH-$C^{\alpha}H$ NOEs are shown inside a box and the (i + 1) NOEs are shown in the

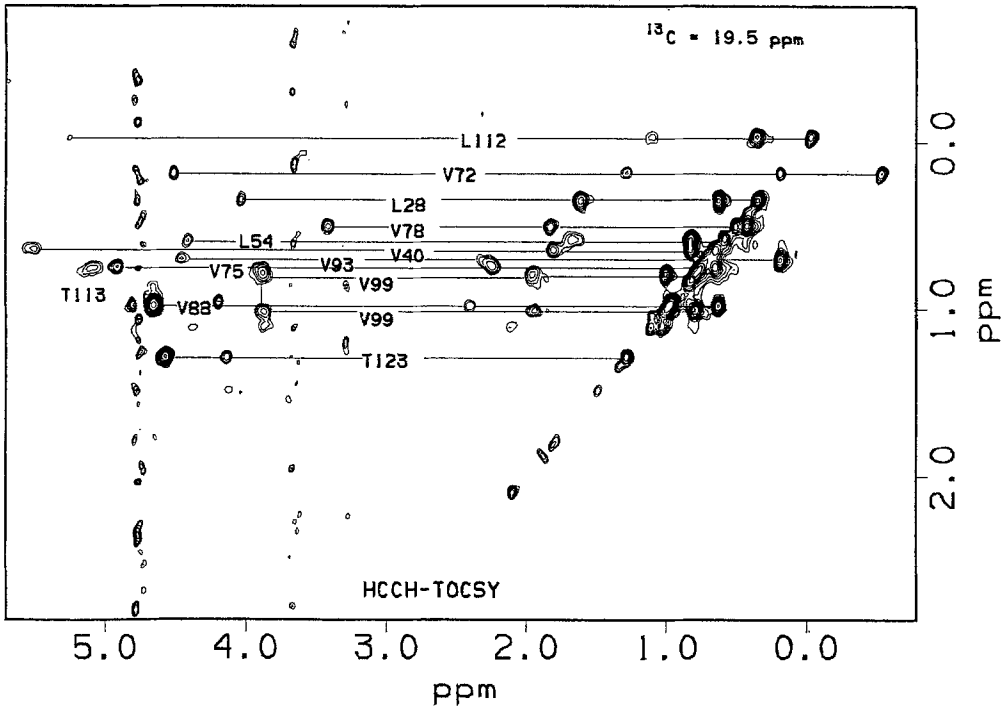

Fig. 2. Plane ($\delta^{13}C$ = 19.5 ppm) from the 3D HCCH-TOCSY spectrum, showing the correlation of various methyl proton resonances with the other side-chain proton resonances. This experiment provided correlation of most of the amino side-chain protons with their respective $C^{\alpha}H$ resonances.

adjacent strip for residues of the βB strand. Residue 39 is a proline and thus is not shown. In the αB helix, the $C^{\alpha}H_i$-$NH_{(i+3)}$ NOEs typical of this secondary structure are also observed. One of the problems associated with the NOE-based assignment method is readily apparent in Fig. 4: the degeneracy or near-degeneracy of resonances can lead to several ambiguities in the assignments. Thus, a single NH-NH cross peak is observed for the α-helical Ala^{29}, Asn^{34} and Thr^{35}. For Ala^{29}, the problem arises from the near-equivalence of the amide resonances of Leu^{28} (7.65 ppm) and Trp^{30} (7.59 ppm). Similarly, Asn^{34} and Thr^{35} have their respective amide resonances at 7.19 and 7.14 ppm. Thus, the HN(CO)CA experiment (based on the large backbone heteronuclear coupling) removes the ambiguity in these cases, where overlapped resonances preclude positive assignment. Figure 5 summarizes the detected sequential and medium-range NOE connectivities as well as the amide exchange rates for the DHFR–folate complex.

A single triple-resonance experiment (HN(CO)CA), which correlates backbone resonances via J-coupling rather than relying on the detection of sequential NOEs, was performed. In this experiment, a cross peak in the 3D matrix is generated at the ^{15}N-$^{1}H(i)$ amide frequency and the C^{α} frequency of residue (i − 1) by virtue of the common coupling of $^{15}N_i$ and C^{α}_{i-1} to the intervening carbonyl (i − 1). The HN(CO)CA experiment, which detected 135 of the expected 149 N_i-to-C^{α}_{i-1} cross peaks, verified the earlier sequential assignments and filled in missing segments of the backbone. Figure 6 shows a slice (^{13}C = 53.6 ppm) from the HN(CO)CA experiment. Thus, by combining the sequential backbone NOE-based assignment method and the triple-resonance

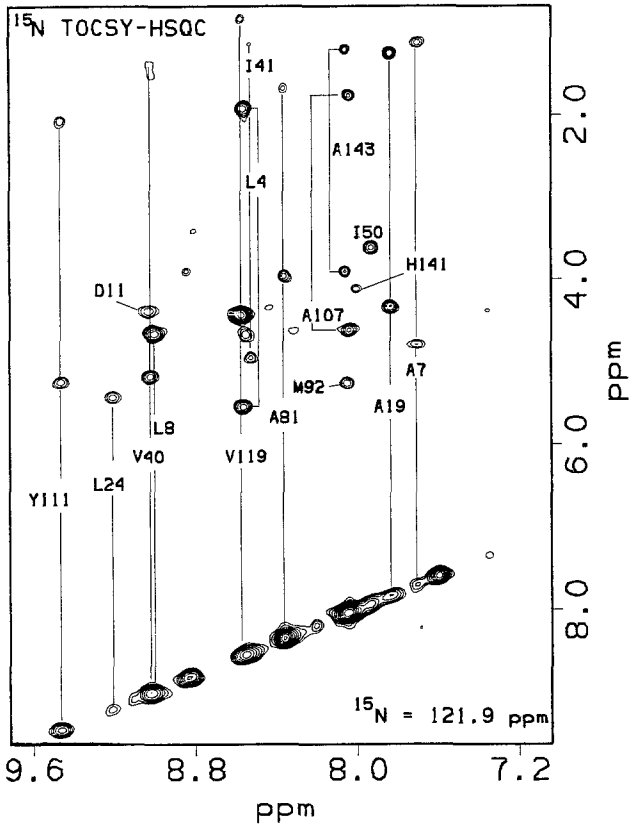

Fig. 3. Plane from the 3D ^{15}N TOCSY-HSQC spectrum (^{15}N = 121.9 ppm), showing the correlations from the backbone amide resonances to their corresponding $C^{\alpha}H$ and $C^{\beta}H$ resonances.

experiment, 95% of the ^{15}NH amide resonances and 90% of the $^{13}C^{\alpha}$ were assigned (Table 1). Figure 5 shows the residues that were sequentially assigned using the HN(CO)CA experiment and the difference in the $^{13}C^{\alpha}$ resonance frequencies ($\Delta\delta$) from the random coil values.

Secondary structure

Figure 5 presents the sequential and medium-range NOEs observed for the DHFR–folate complex. From these, as well as the pattern of slowly exchanging amide resonances and the observed long-range NOEs, it is possible to describe elements of the secondary structure of this binary complex. α-Helices should show a specific pattern of NOEs, typical of this secondary structure; these NOEs include N_iN_{i+1}, α_iN_{i+3} and α_iN_{i+2}. Based on these criteria, Ala^{26} would be the initial residue and Thr^{35} the last residue of the αB helix. Leu^{24} may be the initial residue in this helix (an α_iN_{i+2} NOE is observed), with a proline in position 2, as described in the X-ray crystal structure (Bolin et al., 1982). However, the α_iN_{i+3} NOEs for Ala^{26}–Ala^{29} and Asp^{27}–Trp^{30} are not detected, which may be an indication of some flexibility for the residues at the start of this helix. Except for some possible differences at the Leu^{24} and Pro^{25} positions, the NOEs are consistent with the X-ray structure for this helix. The next helix, αC, is less well defined in terms of NOEs,

but the N_iN_{i+1} stretch of seven residues is consistent with a short α-helical segment. The αE helix shows the typical NOEs from Val[78] to Cys[85], corresponding to the crystal structure designation. The αF helix is better defined, with both α_iN_{i+3} NOEs and α_iN_{i+2} NOEs observed from Arg[98] to Pro[105]; the initial residue may be Gly[97], but it is unassigned in this study. A useful indicator of secondary structure is the C^α secondary shift (Δδ) (Spera and Bax, 1991), which clearly reveals the positions of the α-helices in DHFR. For the four helices, generally a positive shift from their random coil values for the C^α chemical shifts is observed (Fig. 5), consistent with an α-helical geometry for these residues. Coupling constant data, which would potentially define the backbone φ and ψ angles, is not available to confirm the backbone geometry for these α-helices.

The β-strands are characterized by strong α_iN_{i+1} NOEs, slowly exchanging amide resonances, $^3J_{NH\text{-}\alpha H}$ coupling constants greater than 8 Hz (not available), and interstrand long-range NOEs. Except for specific regions and at specific positions, we generally observe strong sequential NOEs

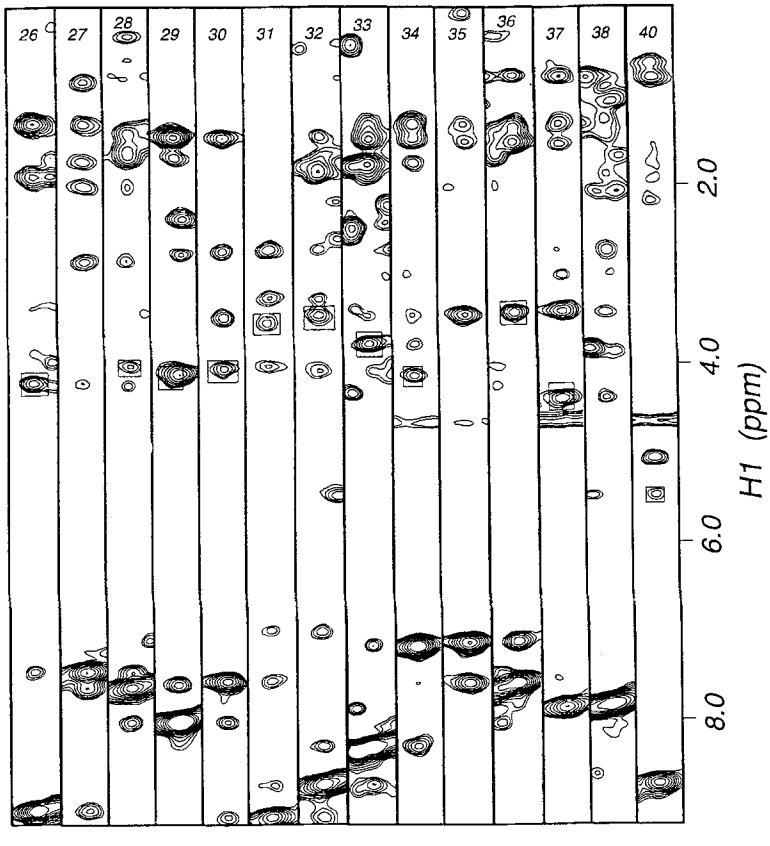

Fig. 4. Strip plots of amide resonances from several planes of the 3D ^{15}N NOESY-HSQC spectrum, showing the sequential and long-range NOEs observed for residues 26–40. Residue 39 is a proline. The intraresidue NH-to-$C^\alpha H$ NOEs are designated with a box. These residues cover the αB helix (24–35) and the βB strand (36–40). Note the $N_iN_{(i+1)}$ NOEs in the helix and the $\alpha_iN_{(i+1)}$ NOEs from residues 36–40. Val[40] shows an NOE to Pro[39] $C^\alpha H$ at 5.07 ppm. The sequential NOEs from 29 to 28 and 29 to 30 are not observed, because of the near-degeneracy of the NH resonances of Leu[28] (7.65 ppm) and Trp[30] (7.59 ppm). Likewise, the sequential $N_iN_{(i+1)}$ NOE from Asn[34] (7.19 ppm) to Thr[35] (7.14 ppm) is not seen.

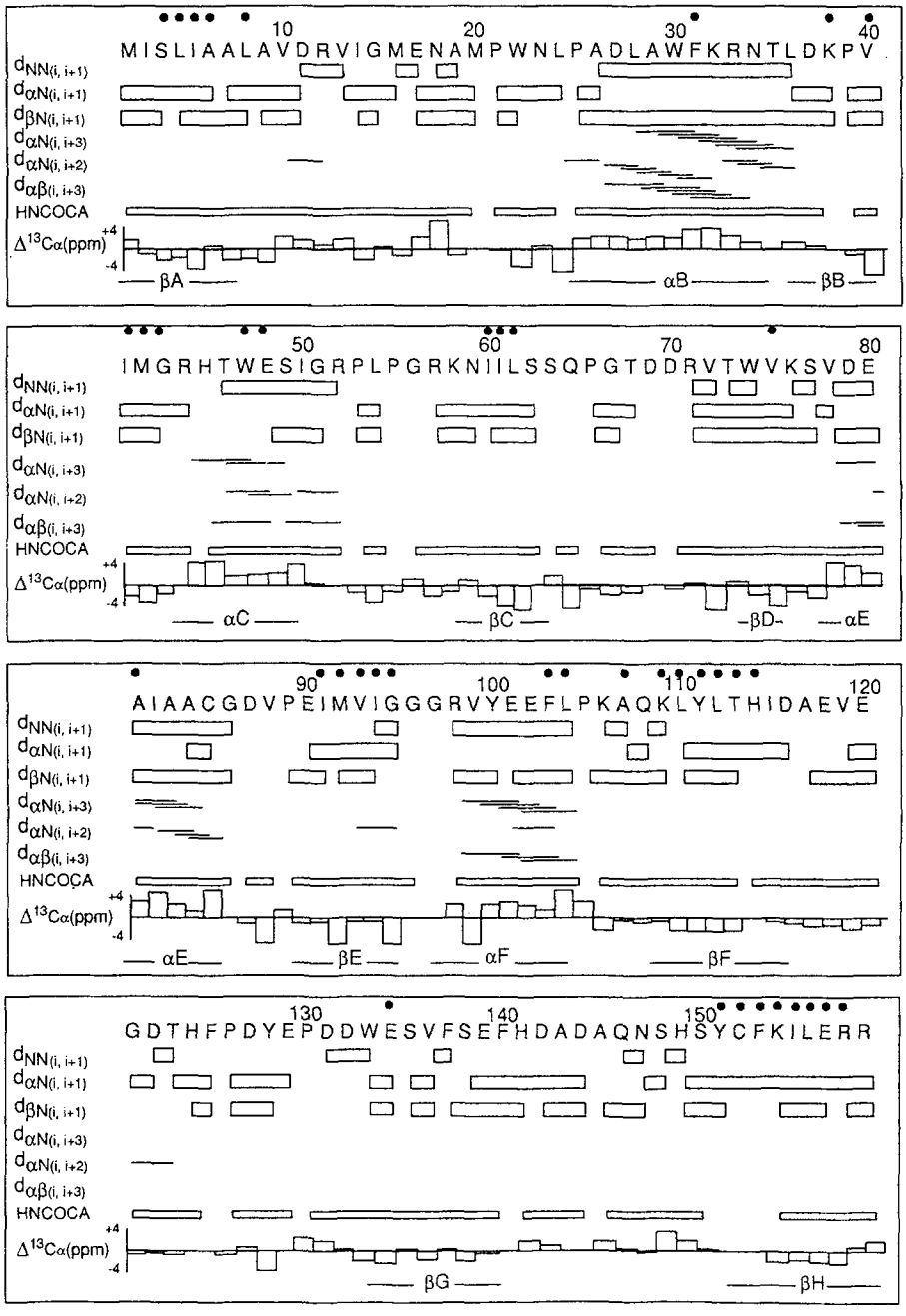

Fig. 5. Summary of the sequential and medium-range NOEs, the slowly exchanging amide protons, the sequential connectivity obtained with the HN(CO)CA experiment, and the difference of the C^{α} chemical shifts from the random coil values observed for the *E. coli* DHFR–folate complex. The solid circles indicate the amide proton resonances which could be detected in a ^{1}H-^{15}N HSQC experiment after 30 h in $^{2}H_2O$ at 303 K. $^{13}C^{\alpha}$ secondary shifts are based on values given by Spera and Bax (1991), with an adjustment of 2 ppm made for referencing differences. The designation of the α-helices and the β-strands follows the nomenclature used in the X-ray crystal structure (Bolin et al., 1982), where the first α-helix is αB as it is after βA in the primary structure.

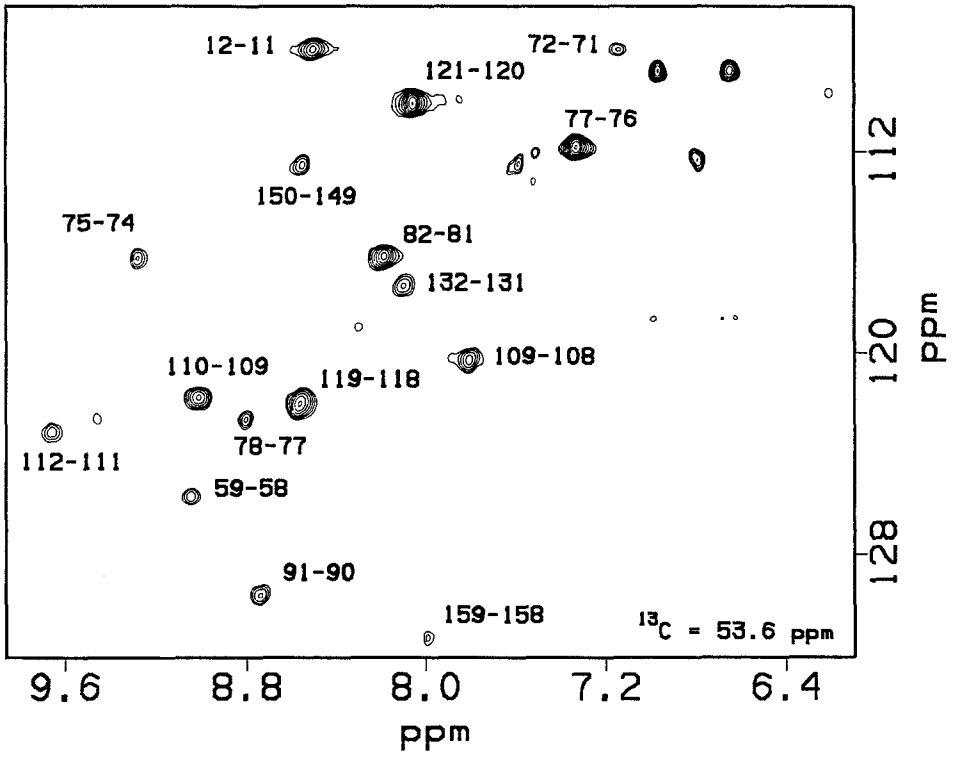

Fig. 6. Plane (^{13}C = 53.6 ppm) from the HN(CO)CA spectrum, showing several of the sequential connectivities. This is not the optimal level for all connectivities shown.

for the residues involved in the β-sheet, as laid out in the X-ray crystal structure (Bolin et al., 1982; Bystroff and Kraut, 1991). For example, Fig. 4 shows the intensity of the $\alpha_i N_{i+1}$ NOEs for the βB strand, a short strand in the eight-stranded β-sheet of DHFR. Both the NH of Leu[36] and Val[40] show strong NOEs to the i − 1 αH resonance. Lys[38] shows the sequential NOE from its amide resonance to Asp[37], but it is weak. However, the intraresidue NH-αH NOE is missing for Lys[38], perhaps indicating some inherent intensity loss for this resonance. Generally, it has been observed for the β-strands of DHFR that the intensity of the $\alpha_i N_{i+1}$ NOEs diminishes as the conformation of the protein changes from the regular extended β-conformation to that of a more irregular loop. In the example of the switch from an α-helix to a β-strand (αB helix to βB strand), as is seen in Fig. 4, the change from $N_i N_{i+1}$ to strong $\alpha_i N_{i+1}$ NOEs is immediate. Also, the long-range interstrand NOEs are consistent with the eight-stranded β-sheet topology found in the solid-state structure, and the secondary C^α shifts ($\Delta\delta$) are consistent with the location of the β-strands in DHFR, with a slight negative deflection on the scale presented in Fig. 5.

Loops generally created the most difficulty in the assignment process, presumably stemming from exchange broadening of the resonances as well as from the increased exchange rate of the amides with the saturated solvent. However, certain segments of the β-strands were also difficult to assign sequentially by using both NOE and backbone J-coupling-based methods. In particular, residues 151–153 were missing both $\beta_i N_{i+1}$ NOEs *and* HN(CO)CA correlation; these residues do

TABLE 1
^{1}H, ^{15}N AND ^{13}C CHEMICAL SHIFTS FOR DIHYDROFOLATE REDUCTASE[a]

Residue	HN	NH	H^{α}	C^{α}	H^{β}	C^{β}	H^{γ}	C^{γ}	Other
Met[1]			4.24	52.3	2.32, 2.42	30.0	2.60, 2.69	27.7	
Ile[2]	9.40	124.6	4.69	58.8	1.97	37.4[b]	1.83[c] (0.93)[d]	(15.6)	1.04 (H^{δ}); 11.4 (C^{δ})
Ser[3]	9.44	125.7	6.01	54.3	3.80, 4.24	63.7			
Leu[4]	8.56	121.9	5.58	51.6	1.93		1.96	27.6	0.99, 1.07 (H^{δ}); 22.6, 23.9 (C^{δ})
Ile[5]	8.67	120.1	6.10	55.8	1.23		2.13, 2.20 (1.03)	(13.5)	0.34 (H^{δ}); 12.2 (C^{δ})
Ala[6]	8.55	126.4	4.78	50.6	0.80	23.2			
Ala[7]	7.70	121.9	4.78	48.1	1.14	17.8			
Leu[8]	9.01	122.8	4.69	51.4			1.28	26.0	0.33, 0.48 (H^{δ}); 23.3, 23.3 (C^{δ})
Ala[9]	8.72	124.6	4.98	47.7	1.70	17.1			
Val[10]	7.80	118.5	3.86	63.0	2.11	29.6	1.03, 1.11	18.6, 20.5	
Asp[11]	9.03	121.8	4.38	54.1	2.92, 3.12	36.9			
Arg[12]	8.50	108.0	3.76	55.3					
Val[13]	6.87	120.6	3.84	62.6	1.83	30.1	0.80, 1.00	18.4, 21.3	
Ile[14]	7.88	119.4	5.01	57.1	2.11	39.0	0.87, 1.47 (1.21)	(15.6)	1.09 (H^{δ}); 11.2 (C^{δ})
Gly[15]	8.64	108.3	3.86, 4.12	43.3					
Met[16]	8.45	119.3	4.62	52.5	1.97, 2.10				
Glu[17]	8.85	122.5	3.91	57.1	2.12, 2.17		2.27, 2.37	33.5	
Asn[18]	8.31	114.8	4.47	51.6	2.84	35.6			
Ala[19]	7.84	121.7	4.33	49.3	1.27	16.9			
Met[20]	7.66	119.3	4.34						
Pro[21]			4.40	61.0	2.01, 2.10				
Trp[22][e]	6.36	114.3	4.95	52.8					10.37 ($N^{\varepsilon}H$); 132.9 (N^{ε})
Asn[23]	9.47	118.9	4.84	51.2	2.71, 2.97	37.8			
Leu[24]	9.22	122.8	5.41	48.8	0.88, 1.78		1.49		0.16, 0.93 (H^{δ}); 24.3, 23.4 (C^{δ})
Pro[25]			4.29	63.3	1.89, 2.37				
Ala[26]	9.04	119.5	4.21	52.9	1.34	16.9			
Asp[27]	7.48	118.6	4.89	54.5	2.05, 2.88				
Leu[28]	7.65	121.3	4.04	55.3	1.43, 1.72	38.0	1.61	24.5	0.35, 0.63 (H^{δ}); 19.8, 22.0 (C^{δ})
Ala[29]	8.04	120.5	4.13	52.7	1.50	15.2			
Trp[30][e]	7.59	123.8	4.06	58.0					10.41 ($N^{\varepsilon}H$); 130.1 (N^{ε})
Phe[31][e]	9.11	123.2	3.58	59.4	2.75, 3.35				
Lys[32]	8.75	123.4	3.47	58.2	1.84, 1.94				2.86 (H^{ε})
Arg[33]	8.32	117.3	3.79	56.8	1.53, 1.79		1.40, 1.45		3.05 (H^{δ}); 41.4 (C^{δ})
Asn[34]	7.19	111.2	4.15	52.2	1.36				
Thr[35]	7.14	107.2	3.91	59.8	3.43	67.3	0.10	17.7	
Leu[36]	7.60	121.9	3.44	54.6	1.39, 1.53	39.9	1.57	23.1	0.81, 0.81 (H^{δ}); 21.7[f] (C^{δ})
Asp[37]	7.88	113.4	4.42	52.4	3.02	34.9			
Lys[38]	7.84	119.3	4.81		1.49				
Pro[39]			5.07	60.0	1.98, 2.21				
Val[40]	8.73	113.9	5.52	54.9	1.81	31.8	0.65, 0.83	19.6, 17.5	
Ile[41]	8.52	121.8	4.96	57.2	1.16	37.8	0.55, 1.31 (0.56)	(14.7)	0.44 (H^{δ}); 12.1 (C^{δ})
Met[42]	9.06	125.1	5.70	49.7					
Gly[43]	8.95	105.8	4.31, 4.91	41.5					
Arg[44]	8.98	119.4	4.00						
His[45][e]			4.47	57.0	3.40, 3.58				
Thr[46]	8.32	121.5	4.03	65.9	4.25	66.6	1.34	18.4	
Trp[47]	8.04	123.5	4.55[e]	57.9					10.19 ($N^{\varepsilon}H$); 127.6 (N^{ε})

TABLE 1
(continued)

Residue	HN	NH	H^{α}	C^{α}	H^{β}	C^{β}	H^{γ}	C^{γ}	Other
Glu^{48}	8.51	117.8	3.40	56.5	1.93, 2.10		2.30, 2.75	34.7	
Ser^{49}	7.69	114.0	4.17	58.8	3.98, 4.04	61.5			
Ile^{50}	7.93	121.7	3.63	63.1	1.46	36.3	0.26, 1.56 (0.56)	(14.6)	0.34 (H^{δ}); 11.1 (C^{δ})
Gly^{51}	7.58	105.1	3.04, 3.65	43.4					
Arg^{52}	6.94	116.2	4.39		1.69, 1.96				
Pro^{53}			4.27	59.8	1.79, 2.00				
Leu^{54}	9.37	126.1	4.42	50.0			1.67	23.6	0.53, 0.83 (H^{δ}); 24.1, 19.2 (C^{δ})
Pro^{55}			4.45	60.4	1.96, 2.29				4.05 (H^{δ})
Gly^{56}			3.75, 3.92	44.1					
Arg^{57}	7.23	118.2	4.42	52.2	1.29				
Lys^{58}	7.37	123.2	4.40	53.8	1.63, 1.71				2.86 (H^{ε})
Asn^{59}	9.05	125.8	4.80	51.3	2.84				6.67, 7.26 ($N^{\delta}H2$); 109.3 (N^{δ})
Ile^{60}	8.85	126.5	4.47	57.5	1.78	37.2	0.78, 1.26 (0.65)	(16.4)	0.68 (H^{δ}); 13.2 (C^{δ})
Ile^{61}	8.82	127.2	4.64	55.7	0.85	34.2	−0.41, 0.03 (0.24)	(15.9)	−0.43 (H^{δ}); 8.5 (C^{δ})
Leu^{62}	8.83	128.8	4.80	50.7	1.68		1.46	25.6	0.59, 0.81 (H^{δ}); 24.0, 21.9 (C^{δ})
Ser^{63}	8.90	119.3	4.83		3.69, 4.06	62.6			
Ser^{64}			4.40	58.2					
Gln^{65}	8.31	121.5	4.67	50.6	1.79, 2.00	26.4	2.33	31.2	
Pro^{66}			4.01	60.6	1.55, 2.12	29.5	1.88	24.9	3.53 (H^{δ}); 47.8 (C^{δ})
Gly^{67}	5.96	107.5	2.06, 2.81	41.4					
Thr^{68}	7.00	107.0	4.18	58.7	4.40	67.3	0.96	18.5	
Asp^{69}	7.50	121.7							
Asp^{70}				52.5					
Arg^{71}	8.87	118.3	4.24	54.9	1.92		2.05		
Val^{72}	7.15	108.0	4.51	56.0	1.29	30.8	−0.53, 0.19	14.0, 19.9	
Thr^{73}	7.73	116.7	4.37	60.6	3.78	68.6	1.11	18.4	
Trp^{74e}	8.84	129.0	5.01	53.9	2.96, 3.42				9.98 ($N^{\varepsilon}H$); 130.4 (N^{ε})
Val^{75}	9.28	116.3	4.90	56.5	2.25	33.4	0.65, 0.75	15.6, 19.7	
Lys^{76}	8.55	115.7	4.90	53.8	1.82, 1.93		1.70, 1.75		1.50 (H^{δ}); 2.95 (H^{ε})
Ser^{77}	7.33	111.9	4.85	53.8	3.88, 4.23	65.5			
Val^{78}	8.81	122.7	3.42	64.5	1.83	28.2	0.42, 0.51	17.7, 19.9	
Asp^{79}	8.36	117.4	4.36	55.4	2.50, 2.60				
Glu^{80}	7.89	120.5	4.05	56.7	2.10, 2.42		2.60, 2.69		
Ala^{81}	8.36	122.4	3.97	53.3	1.69	15.5			
Ile^{82}	8.18	116.3	3.66	63.7	1.94	37.4	1.12, 2.12 (0.93)	(14.1)	1.02 (H^{δ}); 10.8 (C^{δ})
Ala^{83}	8.13	123.7	4.14	52.7	1.50	15.2[g]			
Ala^{84}	8.00	119.0	4.14	51.3	1.50	15.2			
Cys^{85}	7.44	114.3	3.99	59.9	3.33				
Gly^{86}	7.19	103.1	3.80, 3.95						
Asp^{87}				51.2					
Val^{88}	7.25	114.6	4.78	56.1	2.42	29.5	0.64, 0.98	15.0, 19.2	
Pro^{89}			4.36	62.6	1.91, 2.38				
Glu^{90}	7.77	116.8	4.98	53.6	1.71, 1.78				
Ile^{91}	8.74	129.7	3.93	58.9	1.70	39.1	1.62 (0.78)	(15.4)	0.98 (H^{δ}); 11.6 (C^{δ})
Met^{92}	8.06	121.7	5.25	49.5	2.26				
Val^{93}	9.24	124.2	4.45	59.9	2.28	29.8	0.18, 0.71	17.1, 19.7	

TABLE 1 (continued)

Residue	HN	NH	H^{α}	C^{α}	H^{β}	C^{β}	H^{γ}	C^{γ}	Other
Ile^{94}	8.90	118.1	5.61	59.0	2.67	36.9	(0.92)	(14.6)	1.02 (H^{δ}); 12.3 (C^{δ})
Gly^{95}	6.16	105.0	2.41, 4.11	39.6					
Gly^{96}	8.08	108.9							
Gly^{97}									
Arg^{98}			4.21	56.3	1.90		2.00		
Val^{99}	7.36	120.9	3.88	56.4	1.95	29.1	0.79, 1.01	20.0, 19.2	
Tyr^{100}	8.83	118.0	4.38	58.2					
Glu^{101}	8.25	116.6	3.76	57.7	2.20, 2.28		2.27, 2.45	34.1	
Gln^{102}	7.85	115.2	4.03	56.4	2.05, 2.16				
Phe^{103e}	7.86	112.2	4.46	57.6	2.93, 3.11				
Leu^{104}	8.33	123.3	4.33	58.4	1.52, 2.02		1.87	24.8	0.95, 0.95 (H^{δ}); 21.9, 24.1 (C^{δ})
Pro^{105}			4.58	63.6	1.81, 2.49				
Lys^{106}	7.51	112.4	4.45	52.7	1.87				
Ala^{107}	8.04	122.6	4.64	50.0	1.79	18.4			
Gln^{108}	9.27	117.8	4.61	53.3	2.15, 2.43	29.5	2.52, 2.59	32.2	
Lys^{109}	7.81	120.4	5.75	53.9	2.24	34.6			2.77 (H^{ε})
Leu^{110}	9.03	121.8	5.20	50.7	1.40		0.72	22.7	−0.81, 0.58 (H^{δ}); 21.2, 22.1 (C^{δ})
Tyr^{111e}	9.45	121.9	5.24	53.6	2.62, 3.23				
Leu^{112}	9.66	123.3	5.27	50.6	1.44		1.09	23.4	−0.03, 0.36 (H^{δ}); 19.4, 23.2 (C^{δ})
Thr^{113}	8.07	117.4	5.06	57.8	3.90	67.2	0.77	19.7	
His^{114e}	9.17	126.4	4.87	52.3	2.89				
Ile^{115}	9.18	127.9	4.03	58.9	0.77	37.3	−0.12, 0.84 (0.09)	(14.8)	–0.83 (H^{δ}); 10.8 (C^{δ})
Asp^{116}	8.21	129.2	4.72	51.3	2.60, 2.80				
Ala^{117}	8.12	124.8	4.64	48.8	0.99	19.4			
Glu^{118}	8.55	122.6	4.67	53.4	1.95, 2.00		2.11, 2.28	33.9	
Val^{119}	8.58	122.3	4.43	57.6	1.94	32.9	0.83, 0.83	17.8[e]	
Glu^{120}	8.50	125.0	4.43	53.5	1.91, 2.00		2.23, 2.28	33.8	
Gly^{121}	8.06	110.2	3.99, 4.14	42.6					
Asp^{122}	8.24	117.2	4.82	51.7	2.73				
Thr^{123}	8.04	115.3	4.56	59.5	4.13	67.9	1.29	18.7	
His^{124e}	8.77	121.4	5.49	51.8	2.87, 3.19				
Phe^{125e}	9.07	124.8	4.43						
Pro^{126}			4.27	60.6	1.68, 2.18		1.49		3.30 (H^{δ})
Asp^{127}	8.00	117.7	4.29	52.5	2.43, 2.56	39.5			
Tyr^{128e}	7.26	118.3	4.80	52.6					
Glu^{129}	8.92	123.7	4.61		2.17, 2.23				
Pro^{130}			4.43	63.6	2.05, 2.44				
Asp^{131}	8.83	114.2	4.59	53.9	2.62, 2.72				
Asp^{132}	8.10	117.5	4.64	52.3	2.47, 2.92				
Trp^{133e}	7.67	119.4	4.86	53.9	2.89, 3.10				10.25 ($N^{\varepsilon}H$); 127.8 (N^{ε})
Glu^{134}	9.46	122.8	4.69	51.6	1.83, 2.07				
Ser^{135}	9.02	121.0	4.83	56.4	3.91	60.0			
Val^{136}	9.00	121.8	4.68	59.1	2.45	29.9	0.85, 0.95	15.8, 18.5	
Phe^{137e}	7.90	123.3	4.78	56.1	2.67				
Ser^{138}	7.56	119.5	5.25	54.7	3.48, 3.53	62.6			
Glu^{139}	8.67	125.4	4.23	54.0	2.11				
Phe^{140}	8.60	128.7	4.29		2.72, 2.82				6.94 (H^{δ}); 7.19 (H^{ε})

TABLE 1 (continued)

Residue	HN	NH	H^{α}	C^{α}	H^{β}	C^{β}	H^{γ}	C^{γ}	Other
His^{141}[e]	8.01	123.0	4.13	51.8	0.97				
Asp^{142}	8.02	120.3	4.52	51.0	2.41, 2.81				
Ala^{143}	8.06	122.5	3.91	50.3	1.21	16.0			
Asp^{144}	9.07	121.0	4.66						
Ala^{145}	8.11	117.6	4.10	52.3	1.43	15.5			
Gln^{146}	8.08	113.1	4.44	54.4	1.97, 2.04		2.35	32.1	
Asn^{147}	8.32	119.2	5.63	50.5	2.53, 2.93	38.9			
Ser^{148}	8.76	117.4	4.12	59.8					
His^{149}[e]	7.20	119.5	4.81	53.4	2.31, 3.16				
Ser^{150}	8.55	112.6	4.41	56.3	4.04, 4.18	62.1			
Tyr^{151}	7.67	114.9	5.22						
Cys^{152}	8.26	118.6	4.96		2.73				
Phe^{153}[e]	8.39	127.8	5.12						
Lys^{154}	9.77	123.9	5.51	52.5	2.11				
Ile^{155}	8.69	123.9	5.39	57.8	1.69	38.2	0.99, 1.93 (0.44)	14.7	0.68 (H^{δ}); 10.6 (C^{δ})
Leu^{156}	9.22	125.8	5.79	51.1	1.40, 1.71		1.55	26.3	0.62, 0.85 (H^{δ}); 24.2, 23.5 (C^{δ})
Glu^{157}	9.29	119.5	5.39	52.3	1.90, 2.14	31.4	2.32	34.2	
Arg^{158}	8.13	126.8	3.42	54.7	1.39, 1.54				
Arg^{159}	8.00	131.4	4.00	55.9	1.45		1.75		3.14 (H^{δ})

[a] Experimental conditions: 95% H_2O/5% ^2H_2O, 100 mM phosphate, pH 6.8, 303 K. The ^{13}C chemical shifts were determined at 298 K.
[b] The $^{13}C^{\beta}$ of Ile^{2} and Ile^{82} overlap.
[c] For many methylene groups, both CH_2 resonances could not be assigned.
[d] Resonance assignments for $C^{\gamma}H_3$ of isoleucine side chains are indicated in parentheses.
[e] The side-chain assignments for several aromatic residues have been published (Falzone et al., 1990).
[f] The two $^{13}CH_3$ for this side chain cannot be distinguished in the HCCH experiments.
[g] The $^{13}CH_3$ of Ala^{83} and Ala^{84} overlap.

display slowly exchanging amide resonances (observed in ^2H_2O after 30 h at 303 K). These residues are in the hydrophobic cluster which includes Leu^{24}, Trp^{30}, Tyr^{111}, Ile^{115}, Phe^{137}, Tyr^{151}, Phe^{153} and Ile^{155}. Some process, such as the ring flip of a tyrosine (the side chain of Tyr^{151} is difficult to detect in the folate complex) or an exchange phenomenon associated with a destabilization, caused by the β-bulge at residues 136–137 (which displays sequential N_iN_{i+1} and intrastrand NOEs to Ile^{155} and Leu^{156}, consistent with its existence in solution), could be causing the detection problems with the resonances in this region. Clearly, insight will be provided by the backbone dynamics experiments on the binary complex of DHFR.

The conformation of substrate

To provide a sensitive method for detection of possible multiply bound forms of folate and to define more clearly the conformation of substrate in the active site, a 2D ^{13}C HSQC-NOESY spectrum was recorded with unlabeled protein and ^{13}C-labeled substrate in slight excess over the enzyme. For these experiments, a C-7 and C-9 doubly labeled folate was used, with the C-7 position being the important reporter on the environment of the pteridine ring in the active site. These experiments provided an effective means of removing the signals of protons not coupled to ^{13}C. Therefore, the problems associated with detecting low-concentration multiple conformations of folate in the binary complex by ^1H NMR methods alone are alleviated in the ^{13}C HSQC-

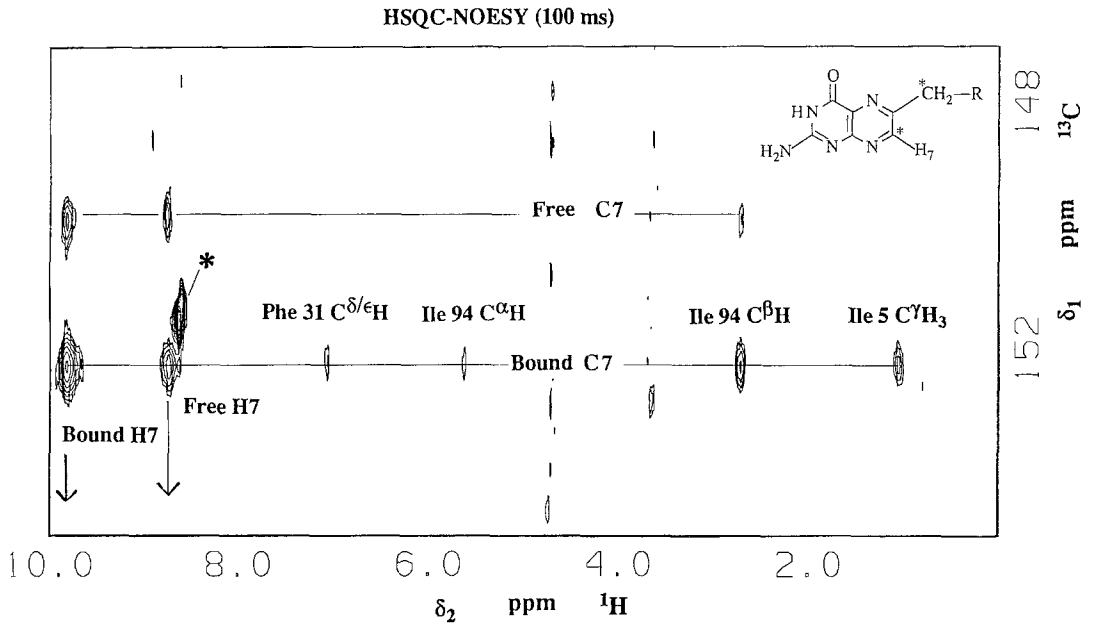

Fig. 7. Region of the 100-ms HSQC-NOESY spectrum, obtained from the complex of ^{13}C-7/^{13}C-9 folate with DHFR (mole ratio 1.3:1). In this region, where the C-7 resonance is found, the only signals detected arise from the free and a single bound form of the ^{13}C-7 on folate. Also indicated in this figure are the NOEs between bound folate and the protein matrix, the exchange cross peaks between the free and bound forms, and the transferred NOEs from the free C-7 resonance. The structure of the pteridine ring of folate is shown in the upper right-hand corner; the labeled carbons are indicated with an asterisk. A cross peak, presumably arising from photocleavage of the pteridine ring with the *p*-aminobenzoyl ring, is indicated by an asterisk.

NOESY experiment with the ^{13}C-labeled substrate. Figure 7 shows a 100-ms 2D ^{13}C HSQC-NOESY with the ^{13}C region near any of the expected bound forms and the free form of ^{13}C-7 plotted. NOEs from C7-H of bound folate to the protein matrix are observed, including those to $C^{\delta}H/C^{\varepsilon}H$ of Phe^{31}, $C^{\alpha}H$ and $C^{\beta}H_3$ of Ile^{94} and the $C^{\gamma}H_3$ of Ile^{5}. The only other resonance found arises from the free ^{13}C-7 and shows a transferred NOE to the $C^{\beta}H_3$ of Ile^{94} and an exchange cross peak to the *single* bound form: no other bound forms can be detected, whether being from an active conformation which would show NOEs to Ile^{5}, Ile^{94} and Phe^{31} or an inactive conformation which has the pteridine ring turned over and displays NOEs to Leu^{28} and a chemical shift similar to H7 on the MTX ring (ca. 8.15 ppm). (A sharp ^{13}C resonance from an impurity is present, presumably from the photocleavage of the substrate, and is marked in the spectrum.)

Single protein resonances were also found in this study of the folate complex. To illustrate this point, examination of Fig. 3 shows a plane (^{15}N = 121.9 ppm) from the ^{15}N TOCSY-HSQC experiment, containing resonances of several residues (Leu^{8}, Ile^{41}, Leu^{110}, Tyr^{111} and His^{141}) that sample two environments in the MTX complex. There is no evidence at this or other ^{15}N chemical shifts for multiple protein conformers. Figure 2 shows a slice (^{13}C = 19.52 ppm) of the HCCH-TOCSY spectrum, with the assignment of residues indicated. Of the resonances in this plane, several were doubled in the MTX complex (Val^{10}, Leu^{54}, Val^{93} and Leu^{112}) but no residues are seen in two environments at this or any other ^{13}C chemical shift.

CONCLUSIONS

The results from the ^{13}C-labeled substrate indicate that the *E. coli* enzyme is unique among the DHFRs studied so far: its two major enzyme conformers both bind the inhibitor MTX and show doubled protein and inhibitor ^{1}H resonances (Falzone et al., 1991), whereas its complex with folate shows single resonances for both substrate (Fig. 7) and protein (see Fig. 1), stemming from the binding of folate by one of the major (the active) protein conformers. Therefore, within the detection limits of both the ^{15}N and ^{13}C experiments, these new results indicate that the folate complex of this enzyme exists in solution predominantly in its active conformation, that is, a conformation poised for reduction by NADPH. Owing to the multiple protein forms that are found in solution for the apoprotein (Cayley et al., 1981; Falzone et al., 1991), the multiple forms exhibited by the *L. casei* DHFR–folate complex (Birdsall et al., 1987), and the similarity of the two bacterial solid-state structures (Bolin et al., 1982), it is remarkable to detect only a single form for the *E. coli* enzyme in the binary folate complex. It is possible that the multiple forms for *L. casei* DHFR are a consequence of its greater tendency to reduce folate than the *E. coli* enzyme. In other words, to reduce both the 5–6 and 7–8 bonds, some substrate flexibility may be required and this is manifested by the multiple folate forms in the *L. casei* protein. Another important difference between *E. coli* DHFR and enzyme from other sources (human and *L. casei*) is that the inhibitor (MTX) binds to two protein conformers with nearly the same affinity and the same general orientation in the active site in the *E. coli* protein (both show NOEs between H7 and Leu^{28} (Falzone et al., 1991)), whereas binding of MTX is observed to only one protein isomer for human (Stockman et al., 1992) or *L. casei* (Carr et al., 1991) DHFR.

The ability of DHFR to bind substrate and inhibitor in very different conformations and the existence of a flexible loop that collapses in the active ternary complex suggest a pliable active site, whose properties can be altered by subtle changes in tertiary structure. Therefore, the small differences in the tertiary structures for the two bacterial enzymes must account for the differential affinities of the two (major) enzyme conformers for the substrate folate. The existence of at least two interconverting conformers in solution, with different affinities for substrate and inhibitor, suggests that there should be structural differences between these forms which are responsible for this behavior. The existence of these and possibly other significantly populated interconverting protein conformers may contribute to the complex multichannel folding mechanism of *E. coli* DHFR (Touchette et al., 1986; Jennings et al., 1993).

ACKNOWLEDGEMENTS

This work was supported by the National Science Foundation, grant DMB 9004707, to C.R.M. and the National Institutes of Health, grants GM 24129 to S.J.B. and GM 36643 to P.E.W.

REFERENCES

Baccanari, D.P., Averett, D., Briggs, C. and Burchall, J. (1977) *Biochemistry*, **16**, 3566–3572.
Bax, A. and Subramanian, S.J. (1986) *J. Magn. Reson.*, **67**, 565–569.
Bax, A., Clore, G.M. and Gronenborn, A.M. (1990a) *J. Magn. Reson.*, **88**, 425–431.
Bax, A., Sklenar, V., Kay, L.E., Torchia, D.A. and Tschudin, R. (1990b) *J. Magn. Reson.*, **86**, 304–318.

Bax, A. and Ikura, M. (1991) *J. Biomol. NMR*, **1**, 99–103.
Birdsall, B., De Graw, J., Feeney, J., Hammond, S., Searle, M.S., Roberts, G.C.K., Colwell, W.T. and Crase, J. (1987) *FEBS Lett.*, **217**, 106–110.
Birdsall, B., Feeney, J., Tendler, S.J.B., Hammond, S.J. and Roberts, G.C.K. (1989) *Biochemistry*, **28**, 2297–2305.
Bolin, J.T., Filman, D.J., Matthews, D.A., Hamlin, R.C. and Kraut, J. (1982) *J. Biol. Chem.*, **257**, 13650–13662.
Bystroff, C. and Kraut, J. (1991) *Biochemistry*, **30**, 2227–2239.
Carr, M.D., Birdsall, B., Frenkiel, T.A., Bauer, C.J., Jimenez-Barbero, J., Polshakov, V.I., McCormick, J.E., Roberts, G.C.K. and Feeney, J. (1991) *Biochemistry*, **30**, 6630–6641.
Cayley, P.J., Dunn, S.M.J. and King, R.W. (1981) *Biochemistry*, **20**, 874–879.
Clore, G.M. and Gronenborn, A.M. (1989) *Crit. Rev. Biochem. Mol. Biol.*, **24**, 479–564.
Cowart, M., Falzone, C.J. and Benkovic, S.J. (1994) *J. Label. Compounds Radiopharm.*, **34**, 67–71.
Drobny, G., Pines, A., Sinton, S., Weitekamp, D.P. and Wemmer, D. (1979) *Symp. Faraday Soc.*, **13**, 49–55.
Falzone, C.J., Benkovic, S.J. and Wright, P.E. (1990) *Biochemistry*, **29**, 9667–9677.
Falzone, C.J., Wright, P.E. and Benkovic, S.J. (1991) *Biochemistry*, **30**, 2184–2191.
Fierke, C.A., Johnson, K.A. and Benkovic, S.J. (1987) *Biochemistry*, **26**, 4085–4092.
Ikura, M., Kay, L.E. and Bax, A. (1991) *J. Biomol. NMR*, **1**, 299–304.
Iwakura, M. and Tanaka, T. (1992) *J. Biochem.*, **111**, 31–36.
Jennings, P.A., Finn, B.E., Jones, B.E. and Matthews, C.R. (1993) *Biochemistry*, **32**, 3783–3789.
Li, L., Falzone, C.J., Wright, P.E. and Benkovic, S.J. (1992) *Biochemistry*, **31**, 7826–7833.
Live, D.H., Davis, D.G., Agosta, W.C. and Cowburn, D. (1984) *J. Am. Chem. Soc.*, **106**, 1939–1941.
Marion, D. and Wüthrich, K. (1983) *Biochem. Biophys. Res. Commun.*, **113**, 967–974.
Marion, D., Driscoll, P.C., Kay, L.E., Wingfield, P.T., Bax, A., Gronenborn, A.M. and Clore, G.M. (1989a) *Biochemistry*, **28**, 6150–6156.
Marion, D., Ikura, M., Tschudin, R. and Bax, A. (1989b) *J. Magn. Reson.*, **85**, 393–399.
Norwood, T.J., Boyd, J., Heritage, J.E., Soffe, N. and Campbell, I.D. (1990) *J. Magn. Reson.*, **87**, 488–501.
Shaka, A.J., Keeler, J. and Freeman, R. (1983) *J. Magn. Reson.*, **53**, 313–340.
Shaka, A.J., Barker, P.B. and Freeman, R. (1985) *J. Magn. Reson.*, **64**, 547–552.
Shaka, A.J., Lee, C.J. and Pines, A. (1988) *J. Magn. Reson.*, **77**, 274–293.
Spera, S. and Bax, A. (1991) *J. Am. Chem. Soc.*, **113**, 5490–5492.
States, D.J., Haberkorn, R.A. and Ruben, D.J. (1982) *J. Magn. Reson.*, **48**, 286–292.
Stockman, B.J., Nirmala, N.R., Wagner, G., Delcamp, T.J., DeYarman, M.T. and Freisheim, J.H. (1992) *Biochemistry*, **31**, 218–229.
Touchette, N.A., Perry, K.M. and Matthews, C.R. (1986) *Biochemistry*, **25**, 5445–5452.
Wüthrich, K. (1986) *NMR of Proteins and Nucleic Acids*, Wiley, New York, NY.